Available online at www.sciencedirect.com
ScienceDirect
Acta Materialia 58 (2010) 373–378
Acta MATERIALIA
www.elsevier.com/locate/actamat

Structural and optical properties of encapsulated ZnO in porous host matrix

Noppadon Sathitsuksanoh [a,*], Dake Wang [b], HongYun Yang [c], Yong Lu [d], Minseo Park [e]

[a] Department of Biological Systems Engineering, Virginia Polytechnic Institute and State University, Blacksburg, VA 24061, USA
[b] Department of Physics, Furman University, Greenville, SC 29613, USA
[c] Department of Chemical Engineering, Auburn University, AL 36849, USA
[d] Department of Chemistry, East China Normal University, China
[e] Department of Physics, Auburn University, Auburn, AL 36849, USA

Received 10 March 2009; received in revised form 6 September 2009; accepted 6 September 2009
Available online 12 October 2009

Abstract

ZnO nanoparticles were encapsulated in the porous activated carbon matrix by incipient-wetness impregnation. The use of the small host matrix allowed the size confinement of ZnO by utilizing the porous nature of the host matrix. Partial fixation of ZnO in the porous matrix determines the size and the dispersion of the particles. Experiments at different calcination temperatures were carried out to investigate structural and optical properties of ZnO nanoparticles in the porous activated carbon matrix using X-ray diffraction, scanning electron microscopy, Raman spectroscopy and photoluminescence. The optimal calcination temperature was found to be ~450 °C in order to confine ZnO nanoparticles in the porous ACP matrix. Near-band-edge UV emission and green emission were both associated with the deep-level defect state. A decrease in full width at half maximum of E_2 mode in Raman spectrum confirmed an increase in crystallite size due to higher calcination temperature, causing an increase in phonon lifetime.

Keywords: ZnO; Nanoparticles; Impregnation; Raman; Photoluminescence

1. Introduction

Semiconductor nanoparticles have been of great interest due to their size constraints, and often exhibit physical and chemical behaviors different from bulk materials [1,2]. The properties of these nanoparticles are expected to be superior to those of bulk materials as there is not only an increase in surface area, but also a reduction in defects, both of which are stabilized in the form of nanoparticles. ZnO is one of the group II–VI semiconductor materials which exhibit promising electronic and optical properties [3]. Recently, ZnO has attracted much interest due to its wide potential applications in UV photonics, transparent electronics, high-frequency piezoelectric devices, luminescent devices, spintronics, non-linear optical devices, and photocatalysis [4,5]. The electronic and optical properties of ZnO nanoparticles can be manipulated by changing grain size [6,7]. Altering the grain size of ZnO nanoparticles offers possibilities for using them in micro-electronic devices [8,9] and biosensors for harmful gases (e.g., SF_6), as well as neutralizers in biological weapons to degrade toxic biochemicals such as naphthalene, antracene, and chlorophenol [10]; all of these potential applications separate them from bulk solid-state counterparts.

Many methods have been employed to synthesize ZnO at nanometer dimensions, such as the electrochemical method, infiltration, vapor deposition, mechanochemical processing, and electrochemical reaction [11–17]; however, most require high temperature and pressure, resulting in high start-up and processing costs and difficulties controlling the ZnO particle size and loading [18]. For example,

* Corresponding author. Tel.: +1 540 231 6615; fax: +1 540 231 3199.
E-mail address: sathino@vt.edu (N. Sathitsuksanoh).

1359-6454/$36.00 © 2009 Acta Materialia Inc. Published by Elsevier Ltd. All rights reserved.
doi:10.1016/j.actamat.2009.09.013

ZnO nanostructures were synthesized at 500 °C on Zn nanoplates [19], 450 °C on the Al_2O_3 substrate covered with a thin layer of ZnO film and/or with NiO as a catalyst [20], 600 °C to decompose $ZnCO_3$ forming ZnO nanoparticles [21], and 550 °C on Si(1 0 0) substrates using a chemical vapor deposition (CVD) [22]. As a result, many efforts have been made for a new nanostructured ZnO synthesis methodology for a low temperature and catalyst-free route. For example, a sol–gel method has been utilized to synthesize ZnO nanostructures using the solution of zinc nitrate hexahydrate and/or methenamine as well as zinc acetate and lithium hydroxide. This method is simple and the operating condition is tailorable depending on the precursors. However, the sol–gel preparation process often requires an additional step to remove the remaining solution from the substrate, which leads to a low crystal quality of ZnO nanostructures. The proposed method in the present study utilizes incipient-wetness impregnation to confine ZnO nanoparticles in a porous host matrix. Incipient-wetness impregnation is often employed in the synthesis of catalysts and adsorbents [23–27]. This method is simple and allows control over particle size by altering temperature and/or pressure.

ZnO nanoparticles, synthesized by incipient-wetness impregnation on porous host materials, take advantage of the porous structure of their substrate matrix. Fig. 1 shows a cross-sectional illustration of porous materials. The porous materials are assumed to be spherical. The surface of porous host materials mainly consists of external and internal surfaces. The latter is generally 100–1000 times higher than the former for macro-porous materials, depending on particle size, pore size, pore distribution, and pore volume [28]. Thus, the selection of host materials plays an important role in the formation of nanoparticles. Oxide host materials such as silica, alumina, activated carbon, and zeolite are commonly used to utilize their micropores (<20 Å) and mesopores (20–500 Å) [29]. A schematic diagram of ZnO nanoparticle formation in the porous structure of the host materials is shown in Fig. 2. Fig. 2a shows a rectangular cross-sectional illustration near the external surface of the porous material. An aqueous zinc precursor can be prepared and then loaded onto the porous host materials (Fig. 2b). The uptake is the sum of the solution occluded in the pores, corresponding in quantity to the total pore volume of the host matrix or slightly less. This allows accurate control over the amount of the active guest materials that will be formed in the pores. The maximum loading obtainable in a single impregnation is limited by the solubility of the precursors. The mechanism of impregnation is simple. It relies on capillary forces to ensure that the salt precursor is drawn into the entire pore structure. Due to capillary pressure, pores are nearly filled, and the dissolution of gas in the liquid assists the process [30].

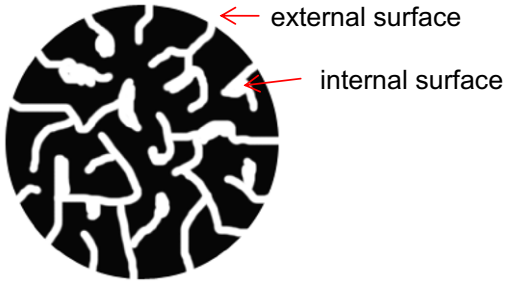

Fig. 1. Schematic representation of a cross-section of the porous host materials.

After impregnation, the materials are usually dried and calcined. Drying is applied to eliminate extraneous solution and unstable anions and cations that have been introduced in the solution from impurities, additives, and stabilizing agents. Moreover, drying causes mixing of the ionic species by diffusion to form a crystal phase. In any case, the resulting materials are in the form of metallic zinc and zinc oxide immobilized on the porous surface (Fig. 2c). Calcination is necessary for undergoing surface diffusion involving surface transport of both zinc and oxygen [31]. In this case, a slow calcination rate is preferred for changes in texture of guest materials toward lower free energies without undergoing larger disturbances. The guest materials immobilized by this method mainly rely on weak van der Waals interactions forming particle aggregates (Fig. 2d). The calcination process affects the grain size of the guest materials, depending on temperature and calcination conditions. Upon calcination, exothermic reactions are developed which lead to excessively high temperatures locally, especially in a nanometer dimension. This affects the activity of ZnO nanoparticles synthesized from diffusion limitation by altering their grain size as well as their optical properties.

ZnO nanoparticles reported here were synthesized by incipient-wetness impregnation on porous host materials. The nature of the small porous host matrix allows the size confinement and loading of ZnO nanoparticles. By controlling the calcination temperature, ZnO nanoparticles can be encapsulated, and the grain domain can be confined. The influence of the calcination temperature on the luminescence of ZnO encapsulated in a porous host matrix to enhance photoluminescence (PL) for the production of stable light-emitting systems was investigated.

2. Experimental details

2.1. Materials

Zinc acetate hexahydrate, ammonia, and ammonium carbonate were analytical grade. They were obtained from Alfa Aesar (Ward Hill, MA). The support host matrix, activated carbon particles of 60 × 90 mesh, was obtained from PICA USA, Inc. (Columbus, OH).

2.2. Synthesis method

Zinc oxide nanoparticles were prepared using a zinc acetate precursor [24], which was loaded onto activated carbon

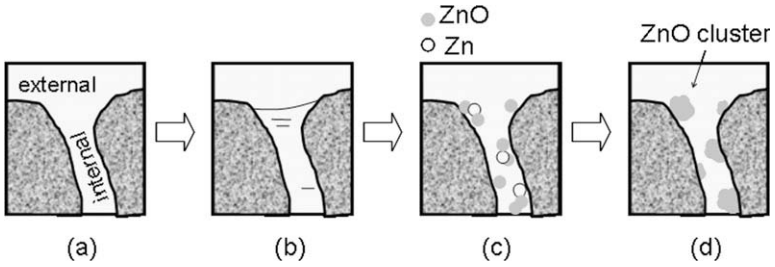

Fig. 2. Schematic illustration of the ZnO cluster formation process in the porous matrix of host materials: (a) porous surface of the host materials; (b) precursor solution drawn into the pore by capillary forces; (c) particle formation after drying; (d) particle aggregation after calcination.

particles (ACP) by incipient-wetness impregnation. The activated carbon particulates were derived from coconut shells, with an average particle size of 150 μm and an average pore diameter of 20 Å, owing to micropores and mesopores confining the growth of the guest materials. This zinc precursor was prepared by adding 70 ml $NH_3{\cdot}H_2O$, 42 g $(NH_4)_2CO_3$, and 66 g $Zn(Ac)_2{\cdot}6H_2O$ into 56 ml deionized water under vigorous stirring. The activated carbon particles were added into an aqueous zinc precursor for 1 h to allow the solution to fill the pores of activated carbon particles. Subsequently, they were vacuum drained to get rid of excess solution prior to drying at 100 °C for 4 h in the vacuum oven. The dry samples were calcined in argon gas for 1 h in a tubular reactor at 250, 350, 450, 600, and 750 °C to observe the change in microstructures.

2.3. Characterization

Inductively coupled plasma mass spectrometry (ICP-MS) was then utilized to confirm the presence of ZnO on a Thermo Jarrell Ash ICAP 61 Simultaneous Spectrometer. The structural phase change and crystallinity of the ZnO nanoparticles at different calcination temperatures were investigated by X-ray diffraction spectroscopy (XRD) using Cu Kα radiation ($\lambda = 1.54056$ Å) with a scanning speed of 4° min^{-1}. The surface morphology of ZnO/ACP particles was observed by scanning electron microscopy (SEM). The optical properties of the ZnO nanoparticles in the porous carbon matrix were studied using Raman scattering and photoluminescence spectroscopy at room temperature. The 325 nm (20 mW) and 441.6 nm (80 mW) lines of a HeCd laser were used for excitation of photoluminescence and Raman spectroscopy, respectively. The excitation light was focused to a spot ~5 μm in diameter. The spectra were collected using the Jobin–Yvon's spectrometer with a thermoelectrically cooled charge coupled device (CCD) detector.

3. Results and discussion

3.1. Influence of temperature on the structure and morphology of ZnO nanocrystal sizes

The diffraction patterns of ZnO nanoparticles synthesized at different temperatures are presented in Fig. 3.

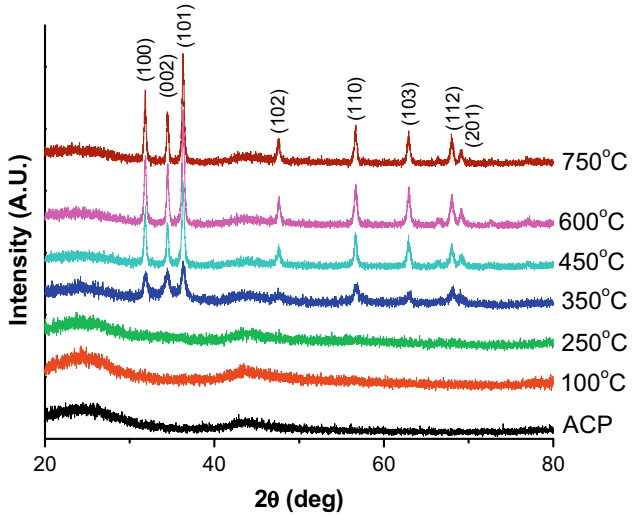

Fig. 3. XRD patterns of ZnO/ACP at different calcination temperatures.

The diffraction peaks of ZnO are not shown in the samples calcined at 100 and 250 °C, but many distinct reflections appear at temperatures higher than 350 °C. These reflections correspond to the hexagonal wurtzite structure of ZnO (JCPDS card No. 36–1451). Su et al. [32] reported the decomposition temperature of zinc acetate to be around 280 °C. As a result, for the synthesis at 100 and 250 °C, the XRD patterns are featureless. No nanocrystals were present. Increasing calcination temperature to 350 °C and above shows a feature of hexagonal wurtzite structure of ZnO as zinc acetate decomposition yielding ZnO. This takes place in three steps [33]:

$$Zn(CH_3COO)_2 \cdot 2H_2O \rightarrow Zn(CH_3COO)_2 + 2H_2O$$
$$4Zn(CH_3COO)_2 + H_2O \rightarrow Zn_4O(CH_3COO)_6 + 2CH_3COOH$$
$$Zn_4O(CH_3COO)_6 \rightarrow 4ZnO + 3CH_3OCH_3 + 3CO_2$$

The ICP-MS analysis and mass balance results indicated the presence of ZnO to be around 18.6 wt.%. A further increase in temperature from 450 to 750 °C results in higher intensities of ZnO reflections. The grain size of these ZnO nanoparticles was then calculated based on (1 0 0) reflection using the Debye–Scherrer equation [34]. The grain size obtained was then plotted as a function of calcination temperature, as shown in Fig. 4. The narrowing of the XRD line-widths with increasing calcination temperature shows

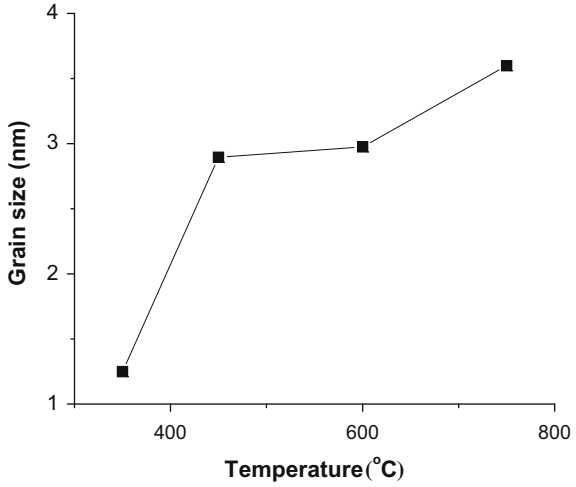

Fig. 4. Relationship between calcination temperature and ZnO grain size.

the increase in crystallite size. The results show that an increase in calcination temperature from 350 to 450 °C causes an increase in grain size [35]. Upon increasing calcination temperature to 600 °C, only a slight change in grain size was observed. A further increase in calcination temperature shows a dramatic increase in grain size.

A change in microstructure of the ZnO nanoparticles in the pores of activated carbon by sintering is a complex process. Initially, the ZnO nanoparticles inside the pores of the activated carbon are transported between particles in close proximity from the higher energy surface to the lower energy surface, causing the area of contact to increase as sintering temperature increases.

We further verified changes in surface morphology of ZnO/ACP at calcination temperatures of 450 and 750 °C by SEM. Results are shown in Fig. 5. Fig. 5a shows an ACP surface morphology prior to ZnO impregnation. It is shown that ACP is porous and consists of a large amount of mesopores and micropores, rendering it a good substrate for ZnO encapsulation. After calcination at 450 °C, ZnO nanocrystals were formed; however, no change in surface morphology was observed, as shown in Fig. 5b. This is due to the confinement of ZnO nanocrystals in the porous ACP. A further increase in calcination temperature to 750 °C showed many small particles precipitating on the external surface of ACP, as shown in Fig. 5c. This phenomenon is believed to take place due to the expansion of the impregnation solution at high temperatures and results in the formation of ZnO on the external surface of ACP. These ZnO nanoparticles on the external surface of the ACP enhance the intensities of ZnO peaks in the XRD, as shown in the higher intensities of ZnO reflections at 750 °C. Compared to those at 450 and 600 °C, the reflections at 750 °C resulted in overestimating the ZnO grain size. Based on XRD and SEM results, we speculate that the optimal calcination temperature has to be ~450 °C in order to confine ZnO nanocrystals in the porous ACP.

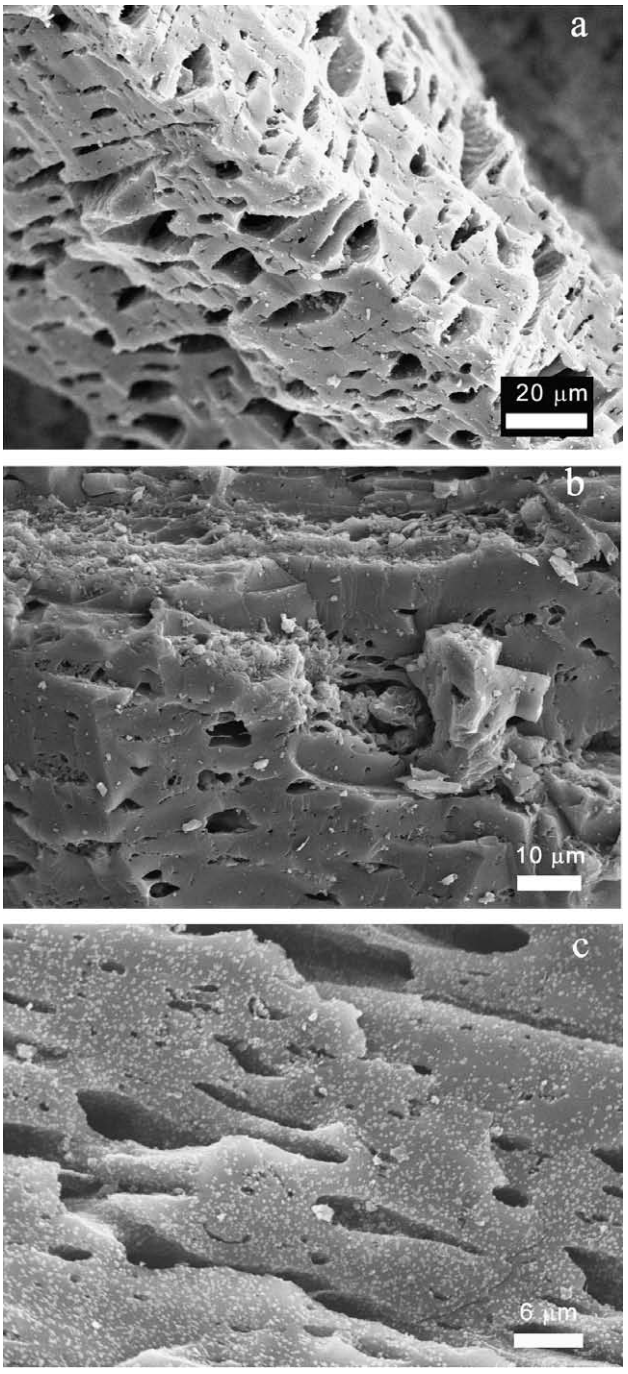

Fig. 5. SEM micrographs of: (a) ACP, (b) ZnO/ACP at 450 °C, and (c) ZnO/ACP at 750 °C.

3.2. The optical properties of ZnO nanoparticles

The room-temperature Raman scattering of ZnO nanoparticles calcined at 250, 450, and 750 °C are presented in Fig. 6. A peak at 438 cm^{-1}, assigned as E_2 mode, and a peak at 585 cm^{-1}, corresponding to the E_{1L} mode, were observed from ZnO nanoparticles calcined at 450 and 750 °C; however, E_2 mode was not observed at 250 °C. The broad and featureless Raman spectrum of the 250 °C material confirms the absence of ZnO nanocrystals. The

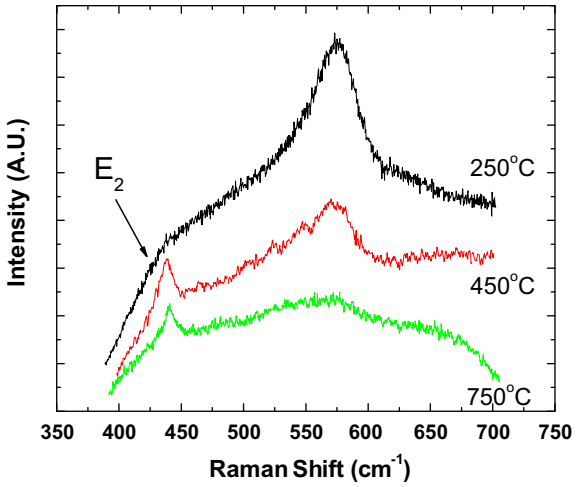

Fig. 6. Room-temperature Raman spectra of ZnO nanoparticles calcined at different temperatures.

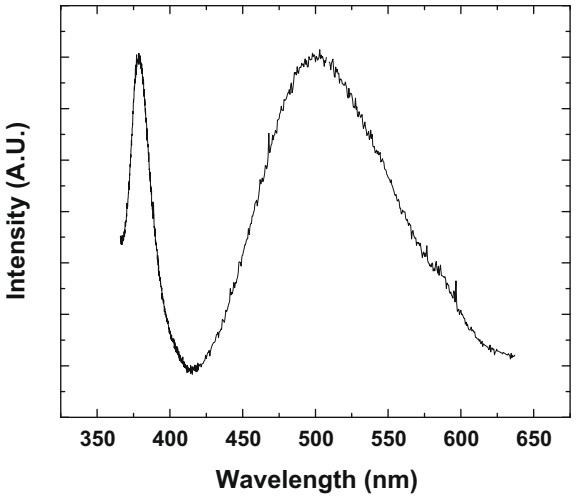

Fig. 7. Room-temperature PL spectrum of ZnO nanoparticles calcined at 450 °C.

presence of the Raman-active optical phonon E_2 mode at 438 cm^{-1} in the spectra is due to the wurtzite hexagonal structure of ZnO. The E_{1L} mode is from the structural defects or impurities, such as oxygen vacancies, zinc interstitials, and free carriers. Based on the XRD spectra, ZnO was not formed at 250 °C. As a result, E_2 mode was not observed. The E_2 modes are clearly seen for ZnO nanoparticles calcined at 450 and 750 °C. The full-width-half-maximum (FWHM) of the E_2 peak is 11 cm^{-1} and 8 cm^{-1} for the ZnO nanoparticles calcined at 450 and 750 °C respectively. A decrease in FWHM of E_2 mode is due to an increase in crystallite size with the calcination temperature [36], which is a primary cause of the increased phonon lifetime. The frequencies of the E_2 peak are 438 cm^{-1} and 441 cm^{-1} for the ZnO nanoparticles calcined at 450 and 750 °C respectively. Wei et al. [37] investigated bulk ZnO single crystal and found that higher temperature annealing improves crystal quality.

The results from the present study were not in agreement with Wei et al.'s findings. This might be due to the nanostructure formation by small crystallites, which causes a change in optical phonons relative to bulk. The slight downshift of the E_2 mode of the sample, calcined at 450 °C, is probably due to the formation of microstructures from small crystallites, compared to that of 750 °C. A smaller particle is more susceptible to laser heating (Raman measurement), thus causing a small shift in the Raman frequencies of the optical phonon relative to bulk. This usually occurs in the case of nanostructures; however, its origin is still unclear [38].

The room-temperature photoluminescence (PL) spectrum of ZnO nanoparticles calcined at 450 °C is presented in Fig. 7. This spectrum shows two distinct luminescence bands: one at 386 nm in the UV region and another at 530 nm corresponding to the green emission. The UV emission is known as a near-band-edge (NBE) emission peak at ~3.28 eV, originating from the recombination of free exciton through an exciton–exciton collision process. A broad green emission band, known as a deep level emission (DPE), relates to the deep-level defect states [22]. The singly ionized oxygen vacancy is responsible for this green emission in the ZnO [39], which results from the recombination of the photogenerated hole with an electron occupying the oxygen vacancy and interstitials of zinc. Owing to the quantum confinement effect, the NBE emission peak is blue-shifted by about 2 nm compared with the NBE emission peak of bulk ZnO crystal.

4. Conclusions

ZnO nanoparticles were prepared by incipient-wetness impregnation using zinc acetate as a precursor. The solution was retained in the activated carbon particulates owing to capillary forces within the porous host matrix. Thermal decomposition allowed ZnO nanoparticle formation and encapsulation in the porous activated carbon matrix. The formation of ZnO nanocrytals was observed at ~350 °C, as zinc acetate decomposed at ~280 °C. An increase in calcination temperature higher than 350 °C caused the growth in grain size of the ZnO nanoparticles and resulted in higher intensities of ZnO reflections. SEM micrographs revealed ZnO precipitation occurs at 750 °C. A change in calcination temperature from 750 to 450 °C exhibited a downshift and a peak broadening in E_2 mode, which is indicative of a higher phonon lifetime. As a result of the small grain size of the nanoparticles, the UV emission in the PL spectrum also displayed a blue-shift compared to that of bulk ZnO crystal.

Acknowledgements

The authors would like to thank Drs. Richard Zallen and Williams Reynolds of Physics and Materials Science and Engineering at Virginia Polytechnic and State University for stimulating and helpful discussions.

References

[1] Park SB, Kang YC. J Aerosol Sci 1997;28:S473.
[2] Li W, Shah S. Encyclopedia of Nanoscience and Nanotechnology, vol. 9. Stevenson Ranch (CA): American Scientific Publishers; 2004. p. 669.
[3] Ying X, Zhang LZ, Tang GQ, Zhang GL, Chen WJ. J Lumin 2004;110:17.
[4] Alivisatos AP. Science 1996;271:933.
[5] Lu Y, Sathitsuksanoh N, Yang HY, Chang BK, Queen AP, Tatarchuk BJ. ACS Symp Ser 2005;914:406.
[6] Kim K-K, Song J-H, Jung H-J, Choi W-K, Park S-J, Song J-H. J Appl Phys 2000;87:3573.
[7] Matsumoto T, Kato H, Miyamoto K, Sano M, Zhukov EA, Yao T. Appl Phys Lett 2002;81:1231.
[8] Clarke DR. J Am Ceram Soc 1999;82:485.
[9] Masaki T, Kim SJ, Watanabe H, Miyamoto K, Ohno M, Kim KH. J Ceram Process Res 2003;4:135.
[10] Pal B, Sharon M. Mater Chem Phys 2002;76:82.
[11] Gies H, Grabowski S, Bandyopadhyay M, Grunert W, Tkachenko OP, Klementiev KV, et al. Microporous Mesoporous Mater 2003;60:31.
[12] Kitano M, Shiojiri M. J Electrochem Soc 1997;144:809.
[13] Mo CM, Li YH, Liu YS, Zhang Y, Zhang LD. J Appl Phys 1998;83:4389.
[14] Rajalakshmi M, Arora AK, Bendre BS, Mahamuni S. J Appl Phys 2000;87:2445.
[15] Suyama Y, Tomokiyo Y, Manabe T, Tanaka E. J Am Ceram Soc 1988;71:391.
[16] Tsuzuki T, McCormick PG. Scripta Mater 2001;44:1731.
[17] Ursaki VV, Tiginyanu IM, Zalamai VV, Masalov VM, Samarov EN, Emelchenko GA, et al. J Appl Phys 2004;96:1001.
[18] Liewhiran C, Seraphin S, Phanichphant S. Curr Appl Phys 2006;6:499.
[19] Kim TW, Kawazoe T, Yamazaki S, Ohtsu M, Sekiguchi T. Appl Phys Lett 2004;84:3358.
[20] Wang LS, Zhang XZ, Zhao SQ, Zhou GY, Zhou YL, Qi JJ. Appl Phys Lett 2005:86.
[21] Yu WD, Li XM, Gao XD. Appl Phys Lett 2004;84:2658.
[22] Wang D, Seo H, Tin C, Bozack M, Williams J, Park M, et al. J Appl Phys 2006;99:113509.
[23] Lu A-H, Schmidt W, Matoussevitch N, Bonnemann H, Spliethoff B, Tesche B, et al. Angew Chem Int Edit 2004;43:4303.
[24] Sathitsuksanoh N, Yang HY, Cahela DR, Tatarchuk BJ. J Power Sources 2007;173:478.
[25] Hufton J, Waldron W, Weigel S, Rao M, Nataraj S, Sircar S. Sorption enhanced reaction process (SERP) for the production of hydrogen. Proceedings of the 2000 U.S. DOE Hydrogen Program Review, NREL/CP-570-28890; US DOE Washington, DC; 2000. Available from: http://www1.eere.energy.gov/hydrogenandfuelcells/pdfs/28890u.pdf.
[26] Ogata A, Einaga H, Kabashima H, Futamura S, Kushiyama S, Kim H-H. Appl Catal B 2003;46:87.
[27] Sheintuch M, Matatov-Meytal YI. Catal Today 1999;53:73.
[28] Cao L. Carrier-bound immobilized enzymes: principles, applications and design. Weinheim: Wiley-VCH; 2005. p. 189.
[29] Lowell S, Shields JE. Powder surface area and porosity. London; New York: Chapman & Hall; 1991. p. 72.
[30] Satterfield CN. Heterogeneous catalysis in industrial practice. Malabar (FL): Krieger Pub; 1996. p. 83.
[31] Rhead G. Trans Faraday Soc 1965;61:797.
[32] Su X, Zhang ZJ, Wang YQ, Zhu MM. J Phys D – Appl Phys 2005;38:3934.
[33] Paraguay F, Estrada W, Acosta DR, Andrade E, Miki-Yoshida M. Thin Solid Films 1999;350:192.
[34] Nuffield EW. X-ray diffraction methods. New York: Wiley; 1966. p. 105.
[35] Garciamartinez O, Rojas RM, Vila E, Devidales JLM. Solid State Ionics 1993;63–5:442.
[36] Doss CJ, Zallen R. Phys Rev B 1993;48:15626.
[37] Wei XC, Zhao YW, Dong ZY, Li JM. J Cryst Growth 2008;310:639.
[38] Kumar B, Gong H, Gosvami NN, Akkipeddi R, O'Shea SJ. Appl Phys Lett 2006;88:093111.
[39] Vanheusden K, Warren WL, Seager CH, Tallant DR, Voigt JA, Gnade BE. J Appl Phys 1996;79:7983.